Multiframe image super-resolution adapted with local spatial information

Liangpei Zhang,[1] Qiangqiang Yuan,[1] Huanfeng Shen,[2,*] and Pingxiang Li[1]

[1]*The State Key Laboratory of Information Engineering in Surveying, Mapping and Remote Sensing, Wuhan University, China*
[2]*School of Resource and Environmental Science, Wuhan University, China*
**Corresponding author: shenhf@whu.edu.cn*

Received September 14, 2010; revised December 15, 2010; accepted December 15, 2010; posted December 16, 2010 (Doc. ID 135083); published February 23, 2011

Super-resolution image reconstruction, which has been a hot research topic in recent years, is a process to reconstruct high-resolution images from shifted, low-resolution, degraded observations. Among the available reconstruction frameworks, the maximum *a posteriori* (MAP) model is widely used. However, existing methods usually employ a fixed prior item and regularization parameter for the entire HR image, ignoring local spatially adaptive properties, and the large computation load caused by the solution of the large-scale ill-posed problem is another issue to be noted. In this paper, a block-based local spatially adaptive reconstruction algorithm is proposed. To reduce the large computation load and realize the local spatially adaptive process of the prior model and regularization parameter, first the target image is divided into several same-sized blocks and the structure tensor is used to analyze the local spatial properties of each block. Different property prior items and regularization parameters are then applied adaptively to different properties' blocks. Experimental results show that the proposed method achieves better performance than methods with a fixed prior item and regularization parameter.

OCIS codes: 100.0100, 100.6640, 100.3020, 100.3190.

1. INTRODUCTION

Super-resolution (SR) refers to the process of obtaining a high-resolution (HR) image or a sequence of HR images from one or a set of low-resolution (LR) observations. SR was first proposed by Tsai and Huang [1] to enhance the resolution of multitemporal Landsat TM images in the frequency domain. After their work, many frequency domain methods were developed in [2–4]. However, the frequency domain methods have some limitations, in that they seldom incorporate prior knowledge, and can only be applied to translation motion models. For this reason, many spatial domain reconstruction methods have been developed in recent decades, including the nonuniform interpolation approach [5,6], iterative back projection (IBP) approach [7–9], projection onto convex sets (POCS) approach [10,11], deterministic regularized approach [12], maximum likelihood (ML) approach [13,14], maximum *a posteriori* (MAP) approach [15], joint MAP approach [16–19], hybrid approach [14], nonlocal-means-based approach [20], and the kernel regression based algorithm [21]. Recently, wavelet domain SR methods have also been proposed [22–25]. Some reviews of the state of the art of SR methods can be found in [26–31].

In this paper, our research is mainly based on the MAP approach, because it is very flexible for the noise model and HR image prior model. Using the MAP framework, the ill-posed SR problem can be successfully represented with a regularization-based least-squares problem, which consists of three parts: a data fidelity item that stands for the noise model, a regularization item that represents the prior model of the HR image, and a regularization parameter that controls the relative contribution of the two items. In the MAP SR model, the prior item plays a very important role in the SR reconstruction process, which guarantees a stable HR estimation. Among the different reconstruction algorithms, many prior models have been proposed, which can be classified into two groups. The first group type is proposed to guarantee the smoothness of the HR image and to suppress noise, such as the GMRF model [32] and the Laplacian model [16]. Although this type of model can reduce noise effectively, it cannot really preserve edge information, and some details are lost. The second group is proposed to preserve edge and detail information, and includes the Huber-MRF model [14], total variation (TV) model [33], and Bilateral total variation (BTV) model [27]. These models have the advantage of preserving edges, but they cannot guarantee the partial smoothness of the HR image in the homogeneous region. As a result, the Huber-MRF model and BTV model may keep some noise, while the TV model may produce staircase effects in the smooth areas. In addition, the regularization parameter is another factor influencing SR reconstruction quality, which controls the perturbation of the solution. If the parameter is too small, edge and detail information will be preserved but noise will be retained; if too large, noise will be eliminated but with the loss of useful edge information. However, most of the SR algorithms use a fixed prior model and regularization parameter for the whole HR image, ignoring the region-dependent property, which cannot produce good results in the smooth regions and edge regions simultaneously.

Thus, we cannot produce a perfect reconstruction result if we use either of the two types of prior model with a fixed regularization parameter for the entire HR image. The region spatial information should be considered to constrain the prior model and regularization parameter, similar with the idea of

the very famous homomorphic filtering algorithm [34] and the Peli-Lim algorithm [35]. In smooth areas, the smoothness-maintaining prior model could be used with a large regularization parameter to suppress noise. In edge areas, the edge-preserving prior model could be used with a small regularization parameter to preserve edge information. To the best of our knowledge, a proper SR reconstruction algorithm considering the region adaptive from both the prior model and regularization parameter aspects has not been proposed.

To overcome the disadvantages of traditional reconstruction models mentioned above, in this paper we propose a block-based region information adaptive reconstruction algorithm, in which the prior model and the regularization parameter are both constrained with spatial information in different regions. The contribution of this algorithm is summarized as follows: Firstl, in order to realize the region adaptive process conveniently and implement the SR rapidly, the target HR image is divided into same-sized blocks. The structure tensor information is then used to identify the spatial properties of each block. Following this, the prior model of each block is adaptively selected with the spatial information. Meanwhile, to realize the region adaptive process of the regularization parameter, a relationship between the regularization parameter and the spatial information is constructed. In smooth areas, a large parameter is selected to maintain partial smoothness. Conversely, a small parameter is selected in the edge areas to preserve edge information. Finally, the SR reconstruction is performed on each block adaptively with its spatial property. There are reasons for dividing the target HR image into blocks and performing the reconstruction on each block. First, reconstruction on each block is faster than on the full image, especially for performance on the large-scale image. Second, for our region spatially adaptive purpose, it is more convenient and computationally cheaper to identify the local spatial information in each block than by a pixelwise region segmentation algorithm for the same purpose [36]. For more information about block-based image processing, please refer to [37–39].

This paper is organized as follows. The observation model and MAP reconstruction model are described in Section 2. In Section 3, our local spatially adaptive algorithm is presented in detail. The optimization method is described in Section 4. In Section 5, some experimental results and discussions are presented and, finally, conclusions are drawn in Section 6.

2. PROBLEM FORMULATION

In this section, we describe the observation model and the MAP solution framework of the SR problem. First, the degradation process from a HR image to a LR image is presented. Then the MAP-based solution model is shown.

A. Observation Model

It is assumed that the HR image is subpixel shifted, blurred, downsampled, and has some additive noise (Fig. 1), and that it produces a sequence of LR images. By far, the most common forward model for the problem of super-resolution is linear, in the form

$$y_k = DB_kM_kx + n_k \qquad k = 1, 2.....p, \tag{1}$$

where x is the original HR image with the size of $l_1M * l_2N$. y_k is the kth LR image, which has the size of $M * N$. l_1 and l_2 are the downsampled factors from row and column, respectively. M_k stands for the warp matrix with size $l_1Ml_2N * l_1Ml_2N$, B_k is the blurring matrix (PSF) with size $l_1Ml_2N * l_1Ml_2N$, and D_k is the downsampling matrix with size $MN * l_1Ml_2N$. n_k is the noise vector with size $M * N$. In this paper, we assume that the blurring matrix B_k and downsampling matrix D_k remain the same between the LR images.

Each LR image has an observation model in the form of function (1). If we incorporate them, the whole observation model could be represented as

$$\left.\begin{aligned} y_1 &= D_1B_1M_1x + n_1 \\ y_2 &= D_2B_2M_2x + n_2 \\ &\vdots \\ y_p &= D_pB_pM_px + n_p \end{aligned}\right\} \rightarrow y = DBMx + n, \tag{2}$$

where $y = [y_1, y_2 \ldots y_p]^T$, $M = [M_1, M_2 \ldots M_p]^T$, $B = [B_1, B_2 \ldots B_p]^T$, $D = [D_1, D_2 \ldots D_p]^T$, and $n = [n_1, n_2 \ldots n_p]^T$.

B. Maximum *a posteriori* (MAP)-Based Solution Model

Using the MAP model, and assuming that the noise is zero-mean Gaussian noise and each LR frame is independent, the solution model of the SR problem can be represented by the following regularization-based least-squares problem:

$$\hat{x} = \arg\min\{\|y - DBMx\|_2^2 + \lambda U(x)\}. \tag{3}$$

In Eq. (3), $\|y - DBMx\|_2^2$ is the data fidelity item, which stands for the fidelity between the observed LR image and the original HR image, and $U(x)$ is the prior item. λ is the regularization parameter, which controls the trade-off between the data fidelity and prior item. The formation of $U(x)$ in our paper will be presented in detail in Section 3.

3. LOCAL SPATIALLY ADAPTIVE SUPER-RESOLUTION (SR)

The prior item $U(x)$ and regularization parameter λ in (3) play a very important role in the SR reconstruction process. They control the perturbation of the solution, solve the ill-posed problem for SR reconstruction, and guarantee a stable HR estimation. However, as shown in the introduction section, the state-of-the-art methods usually employ a fixed prior item and regularization parameter to the whole HR image, not considering the local spatial information differences of the HR image. This approach cannot deliver good results in the

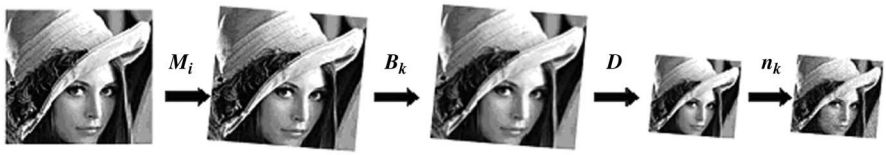

Fig. 1. Degradation process of the HR image.

smooth regions and edge regions simultaneously. Therefore, in our reconstruction framework, we first divide the target image into same-sized blocks, and perform the reconstruction of each block with different prior models and regularization parameters related to the local spatial property of each block.

In this section, our local spatially adaptive SR method is presented. First, the local spatial information analysis using the structure tensor method is described. Next, the selection process of the prior item, dependent on the local spatial information, is shown. Then, the local spatially adaptive mechanism of the regularization parameter is set out. Last, the deblock mechanism to reduce the spatial discontinuity as a result of the block based processing is introduced.

A. Structure Tensor-Based Spatial Property Analysis

The matrix field of the structure tensor, introduced by Forstner and Gulch [40] as well as by Bigun and Granlund [41] in an equivalent formulation, plays a fundamental role in image processing and computer vision. The structure tensor is a powerful tool to discriminate edge information [42]. Consequently, we use it to identify the spatial property of each block. For each pixel of the block, the structure tensor matrix is defined as

$$S(x,y) = \nabla I(x,y)\nabla I(x,y)^T, \tag{4}$$

$$\nabla I(x,y) = \begin{bmatrix} G_x \\ G_y \end{bmatrix}, \tag{5}$$

where G_x and G_y stand for the gradient information of each pixel in the x and y directions. Thus, we can define the structure tensor matrix of a block b_m as

$$S_m = \frac{1}{n}\sum_{i=1}^{n} S_i(x,y) = \frac{1}{n}\sum_{i=1}^{n} \nabla I_i(x,y)\nabla I_i(x,y)^T$$
$$m = 1 \ldots t_m, \tag{6}$$

where n is the number of pixels in each block. t_m is the total number of the block. $S_i(x,y)$ and $\nabla I_i(x,y)$ stand for the structure tensor matrix and gradient information of each pixel. With the structure tensor information, the spatial property parameter δ_m of each block can be defined with the two eigenvalues λ_1^m and λ_2^m of the structure tensor matrix S_m:

$$\delta_m = |\lambda_1^m| + |\lambda_2^m|. \tag{7}$$

Using the parameter δ_m, with a suitable threshold value T, the blocks can be classified into smooth blocks, which stand for the smooth regions, and nonsmooth blocks, which stand for the edge regions. The spatial property of each block can then be used to constrain the setting of the prior item and regularization parameter.

B. Local Spatially Adaptive Prior Model Selection

With the spatial property analysis of each block, the prior model can be selected with the local information as follows:

For the smooth area blocks, to retain the partial smoothness of an HR image, the Laplacian prior model is used in (3) to reconstruct the smooth areas, which has the form

$$U(x)_{\text{smooth}} = \|Qx\|_2^2. \tag{8}$$

Q represents a linear high-pass operation that penalizes the estimation that is not smooth, which is chosen as a two-dimensional Laplacian model in this paper.

For the edge area blocks, to preserve the edge information of an HR image, the Huber-MRF prior model is used in (3) to reconstruct the edge areas, which has the form

$$U(x)_{\text{edge}} = \sum_{i,j}\sum_{c\in C}\rho(d_c(x_{i,j})). \tag{9}$$

c is a local group of pixels contained within the set of all image cliques C. $d_c(x_{i,j})$ is a spatial activity measure for the pixel, which is often formed by first-order or second-order differences. $\rho(.)$ is the potential function, which is selected to be the Huber function in this paper

$$\rho(x) = \begin{cases} x^2 & |x| \le \mu \\ 2\mu|x| - \mu^2 & |x| > \mu \end{cases}, \tag{10}$$

where μ is a threshold parameter, which separates the quadratic and linear regions. Figure 2 shows a typical curve of the Huber function.

As for $d_c(x_{i,j})$, we compute the following finite second-order differences in four adjacent cliques for every location (i,j) in the SR image:

$$\begin{matrix} x_{i-1,j-1} & x_{i-1,j} & x_{i-1,j+1} \\ x_{i,j-1} & x_{i,j} & x_{i,j+1} \\ x_{i+1,j-1} & x_{i+1,j} & x_{i+1,j+1} \end{matrix} \rightarrow \begin{cases} d_c^1(x_{i,j}) = x_{i-1,j} - 2x_{i,j} + x_{i+1,j} \\ d_c^2(x_{i,j}) = x_{i,j-1} - 2x_{i,j} + x_{i,j+1} \\ d_c^3(x_{i,j}) = \frac{1}{\sqrt{2}}(x_{i-1,j-1} - 2x_{i,j} + x_{i+1,j+1}) \\ d_c^4(x_{i,j}) = \frac{1}{\sqrt{2}}(x_{i-1,j+1} - 2x_{i,j} + x_{i+1,j-1}) \end{cases}. \tag{11}$$

C. Local Spatial Information Adjusted Regularization Parameter

The regularization parameter α plays an important role in the reconstruction process. It controls the trade-off between the data fidelity item and the prior model item in function (3), which is also locally dependent. A small α sharpens edges while amplifying noise in the estimated HR image; a large α helps to suppress noise while smoothing edges and the

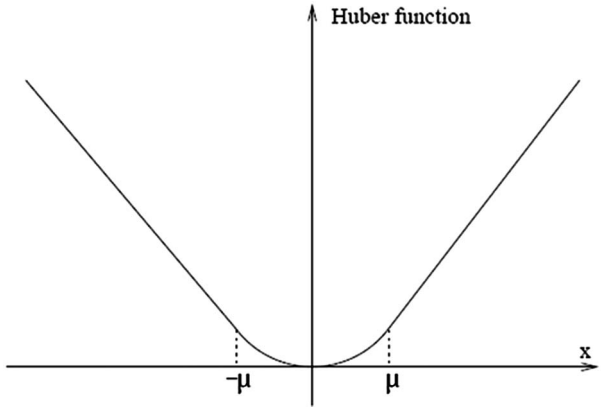

Fig. 2. Curve of the Huber function.

detailed information of the estimated HR image. Figure 3 shows the reconstruction results of too large and too small a regularization parameter.

From the information described above and Fig. 3, it can be seen that if we use a fixed regularization parameter for the entire image, a good result cannot be obtained. Therefore, for smooth areas, a large regularization parameter should be selected to suppress noise. Conversely, a small regularization parameter should be selected in the nonsmooth areas to preserve the edge information.

To realize the local spatially adaptive process of the regularization parameter, we propose to construct a relationship between the regularization parameter and the spatial parameter δ_m of each block. The relationship is presented as

$$\alpha(\delta_m) = \frac{c}{\delta_m + \varepsilon}, \tag{12}$$

where c is a positive constant parameter. ε is a constant, which prevents δ_m from being zero, and is set to be 1 in this paper.

From the function (12), in the smooth area, the smooth parameter will be small, which leads to a large regularization parameter with the purpose of suppressing noise. Conversely, in the edge area, the smooth parameter will be large, which leads to a small regularization parameter with the purpose of preserving edges.

D. Deblock Mechanism

Because the visual discordance may appear at the edge area between different blocks enhanced by different prior information and regularization parameters, we use overlap between different blocks to overcome this problem. More concretely, we apply different a regularization item and parameter to a larger part of the image, then crop the central part and use it as the result. In Fig. 4, the area inside of the solid line is saved as the reconstruction result.

4. OPTIMIZATION PROCEDURE

Using the local spatially adaptive prior model and regularization parameter, for each block of the HR image, the reconstruction model can be written as

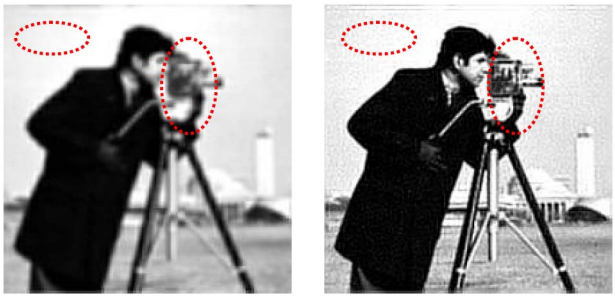

(a) (b)

Fig. 3. Reconstruction with different fixed regularization parameters. (a) Regularization parameter that is too large. (b) Regularization parameter that is too small.

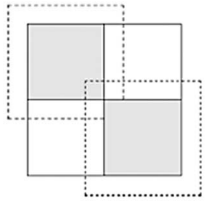

Fig. 4. Deblock mechanism.

$$\hat{x} = \arg\min\left\{ \|y - DBMx\|_2^2 + \begin{cases} \alpha(\delta_m)\|Qx\|_2^2 & \text{if} \delta_m \le T \\ \alpha(\delta_m)\sum_{i,j}\sum_{c\in C}\rho(d_c(x_{i,j})) & \text{if} \delta_m > T \end{cases} \right\}. \tag{13}$$

A gradient descent procedure is designed to minimize the cost function (13). Differentiating the function (13) with respect to x, we have

$$-M^T B^T D^T (y - DBMx) + \alpha(\delta_m)\gamma' = 0, \tag{14}$$

where γ' is the derivative of the local spatially adaptive regularization term that can be solved on a pixel-by-pixel basis. Thus, the HR image is solved using successive approximations iterations

$$x^{n+1} = x^n - \beta^n r^n \quad r^n = -M^T B^T D^T (y - DBMx_n) + \alpha(\delta_m)\gamma', \tag{15}$$

where x^n and x^{n+1} are the HR images of nth and $n+1$th iteration, respectively, and n is the iteration number. In this paper, the analytical solution of the step size β^n is solved as [15,43,44]

$$\beta^n = \frac{(r^n)^T r^n}{(r^n)^T W (r^n)}, \tag{16}$$

where W is the Hessian matrix of the cost function (13). The iteration is terminated when

$$\frac{\|x^{n+1} - x^n\|^2}{\|x_n\|^2} \le d. \tag{17}$$

5. EXPERIMENTAL RESULTS AND DISCUSSION

In this section, we present two simulated data experiments under different noise conditions and an experiment with real data sets to illustrate the performance of the proposed algorithm. To assess the relative merits of the proposed methodology, we compare the proposed algorithm with the bilinear interpolation (BI) results, reconstruction results using the Laplacian prior model and Huber-MRF prior model in the simulated experiments, while adding the comparison of the bicubic interpolation results in the real data experiment.

Dewarping (registration) is a very important and difficult process in SR reconstruction. Because our research focuses on the local spatially adaptive SR, we do not pay much attention to this topic. To better validate the advantage of our proposed local spatially adaptive SR algorithm, the blur and motion parameters are assumed to be known in the first two simulated experiments, and the well-performed registration approach proposed in [45] is used in the real data

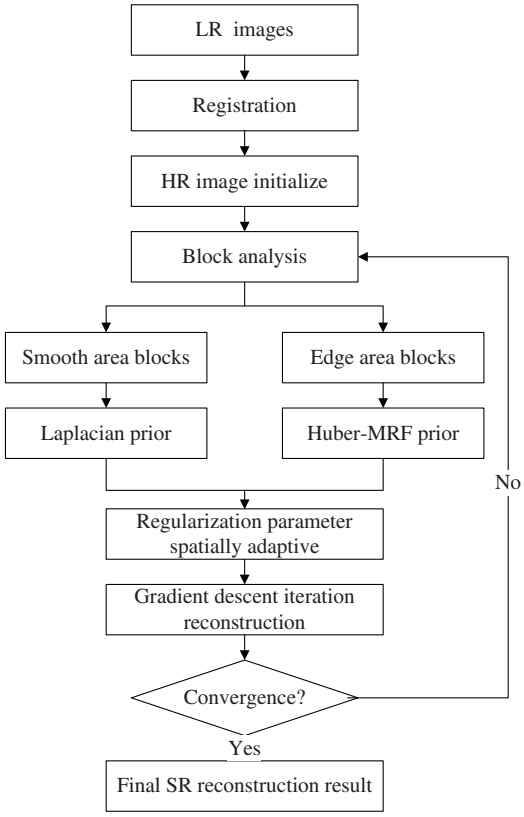

Fig. 5. Flow chart of our reconstruction framework.

experiment 3. The translation motion model is used in all three experiments in this paper.

The block analysis unit of all experiments was $5 * 5$, and the reconstruction factor was set to be 2. The termination condition d in all three experiments was set to be 10^{-6}. The regularization parameter λ in the Laplacian prior model and the Huber-MRF prior model was adjusted until the most visually appealing result was produced, and the same operation was carried on the parameter c in Eq. (12). The flow chart of our reconstruction framework is shown in Fig. 5.

Table 1. MSE and SSIM Values of Different Reconstruction Methods in the First Experiment

Assessment Index	BI	Laplacian	Huber-MRF	Proposed LSA
MSE	628.625	245.819	224.274	213.905
SSIM	0.74931	0.76722	0.84012	0.90499

We use the mean square error (MSE) and the structural similarity (SSIM) to evaluate the reconstruction results. The MSE is usually employed to evaluate the gray value similarity, and the SSIM proposed by Wang *et al.* [46] is used to evaluate the structural similarity. Their expressions are as follows:

$$\mathrm{MSE} = \frac{1}{N}\|\hat{x} - x\|^2, \tag{18}$$

$$\mathrm{SSIM} = \frac{(2\mu_x\mu_{\hat{x}} + C_1)(2\sigma_{x\hat{x}} + C_2)}{(\mu_x{}^2 + \mu_{\hat{x}}{}^2 + C_1)(\sigma_x{}^2 + \sigma_{\hat{x}}{}^2 + C_2)}, \tag{19}$$

where x represents the original HR image, and $\hat{x}$ represents the reconstructed HR image. N is the size of the HR image. μ_x and $\mu_{\hat{x}}$ represent the average gray values of the original HR image and the reconstructed result, respectively. σ_x and $\sigma_{\hat{x}}$ represent the variance of the original HR image and the reconstructed image, respectively, and $\sigma_{x\hat{x}}$ represents the covariance between the original HR and the reconstructed image. C_1 and C_2 are two constants that prevent unstable results when either $\mu_x{}^2 + \mu_{\hat{x}}{}^2$ or $\sigma_x{}^2 + \sigma_{\hat{x}}{}^2$ is very close to zero.

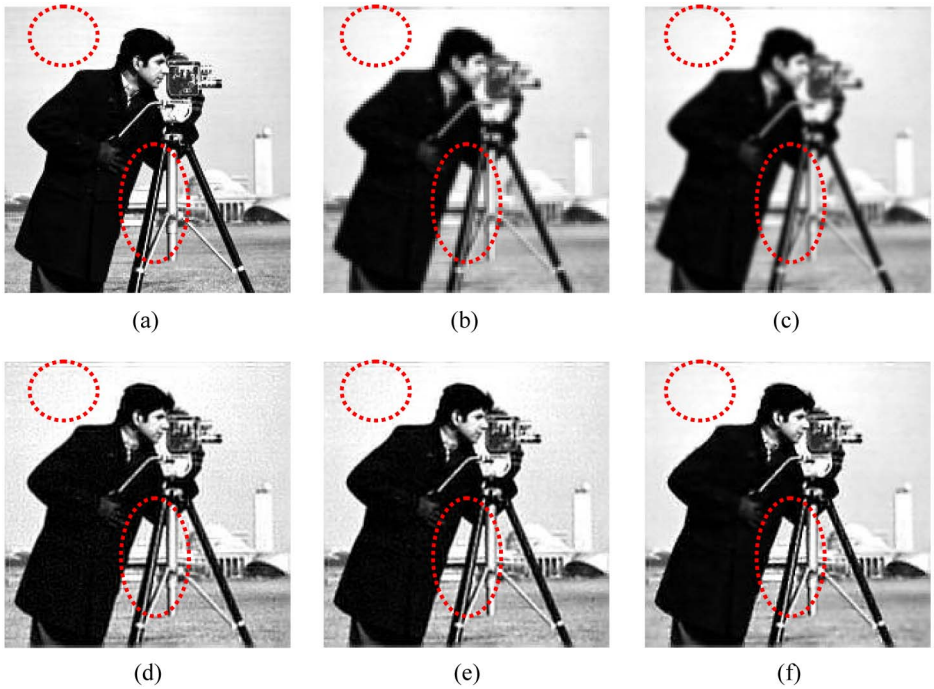

Fig. 6. (Color online) Reconstruction results of the first experiment. (a) Original HR image. (b) LR image. (c) Bilinear interpolation. (d) Laplacian prior result. (e) Huber-MRF prior result. (f) Proposed LSA result.

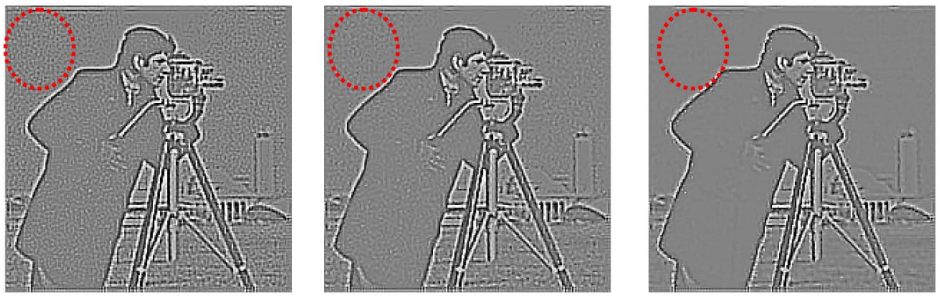

(a) (b) (c)

Fig. 7. (Color online) Edge extraction results of the first experiment. (a) Laplacian prior result. (b) Huber-MRF prior result. (c) Proposed LSA result.

A. Experimental Results

In the first experiment, the original HR image is the "cameraman" image, with size of $200 * 200$ pixels. With the degradation mode described in Section 2, the HR image was first shifted with subpixel displacements to produce four images. Then the sequence was convoluted with a PSF of $5 * 5$ window size and unit variance, and downsampled by a factor of 2 in both the vertical and horizontal directions. Finally, zero-mean Gaussian noise with 0.01^2 variance was added to the sequence.

The reconstruction results of the first experiment are presented in Fig. 6: (a) is the original HR image; (b) is one of the downsampled LR images; (c) shows the bilinear interpolation result. The reconstruction results of the Laplacian prior, the Huber-MRF prior, and the proposed local spatially adaptive (LSA) method, respectively, are shown in Figs. 6(d)–6(f). The MSE and SSIM values of the different methods are presented in Table 1.

Clearly, the proposed local spatially adaptive reconstruction method shows better results than the Laplacian prior and the Huber-MRF prior, which do not consider the constraint of the local spatial information. In the smooth region, the noise is suppressed effectively; in the nonsmooth region, the edge information is better preserved. The effectiveness of the proposed method can also be illustrated with quantitative evaluation results using MSE and SSIM. It is clearly seen from Table 1 that the proposed method has the lowest MSE value and the highest SSIM value, which shows that the proposed method can better maintain both the gray levels and the structural information of the original HR image.

To further present the partial smoothness-maintaining property of the proposed method, we use the $3 * 3$ Gaussian-Laplacian kernel to detect the edge information of the reconstruction results. The detection results are shown in Figs. 7(a)–7(c). It is clearly seen that noise is almost completely suppressed in the smooth region in the local adaptive approach result. However, the noise still seems obvious in the smooth region when using the Laplacian and Huber-MRF priors and a fixed regularization parameter only, because of no consideration being given to the local spatial information constraint.

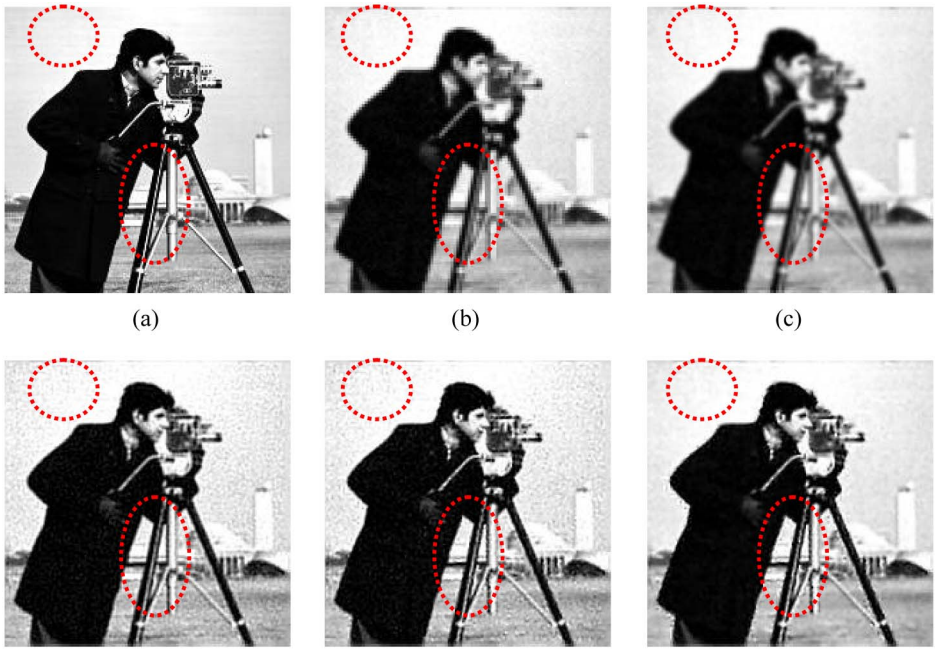

(a) (b) (c)

(d) (e) (f)

Fig. 8. (Color online) Reconstruction results of the second experiment. (a) Original HR image. (b) LR image. (c) Bilinear interpolation. (d) Laplacian prior result. (e) Huber-MRF prior result. (f) Proposed LSA result.

Table 2. MSE and SSIM Values of Different Reconstruction Methods in the Second Experiment

Assessment Index	BI	Laplacian	Huber-MRF	Proposed LSA
MSE	637.174	338.589	332.299	297.531
SSIM	0.67349	0.67449	0.68448	0.83686

The original image and degradation parameters in the second simulated experiment were the same as in the first experiment, except that the variance of the degradation noise was set to 0.05^2.

The reconstruction results of the second experiment are shown in Figs. 8(a)–8(f). Table 2 presents the quantitative evaluation results. Clearly, the proposed method performs robustly with the increase of noise, and suppresses the noise more thoroughly, producing the lowest MSE value and highest SSIM value in the quantitative evaluation results.

In the third experiment, the "Surveillance" video sequence obtained from the Multidimensional Signal Processing (MDSP) Research Group at UCSC [47], used to access the performance of the proposed algorithm, consisted of 15 frames of size $66 * 76$. In order to reduce the computational load, we just selected the first seven frames in our experiment.

The reconstruction results using the real data sets are shown in Fig. 9: (a) is one frame of the "Surveillance" video, in which the block noise as a result of compression is clearly seen; (b) and (c) are the bilinear and bicubic interpolation results; the reconstruction results using Laplacian and Huber-MRF are shown in (d) and (e); (f) presents the proposed local information adaptive reconstruction result. It is clearly illustrated from the result that the proposed method suppresses the compression noise in smooth regions more efficiently without losing the edge information. However, compression noise is evident in the other two reconstruction results,and the "edge" information is processed too aggressively.

B. Discussion

To show the effect of the block size on the reconstruction results, we plot the change of the MSE value versus the block size in the first experiment, which is shown in Fig. 10(a), and the computation time versus the block size, shown in Fig. 10(b). From these two plots, it is seen that with the increase in the block size from $5 * 5$ to $20 * 20$, the MSE value shows only a slight decrease and is maintained with almost no change. However, with the increase in the block size, the computation time increased sharply, because the degradation matrix of each block becomes larger and more time is required to solve the ill-posed function of each block. In the experiment, the SR algorithm was performed using C++ language on common PC platform. Using different programming language (e.g., MATLAB) and/or different hardware configuration, Fig. 10(b) may be different, but it will present the same trend.

From the discussion above, we conclude that an adequate solution is to use a small block size in the reconstruction process, with the purpose of reducing computation time, and meanwhile, it is more reasonable to analyze the local spatial property in a small block area.

The threshold parameter T, which distinguishes the smooth area and edge area, has an important effect on the reconstruction result. If it is too small, a smooth region will be identified as a nonsmooth region, which will lead to the noise not being fully suppressed in the smooth region. Conversely, if it is too large, the nonsmooth regions will be identified as smooth regions, and the edge information cannot be fully preserved.

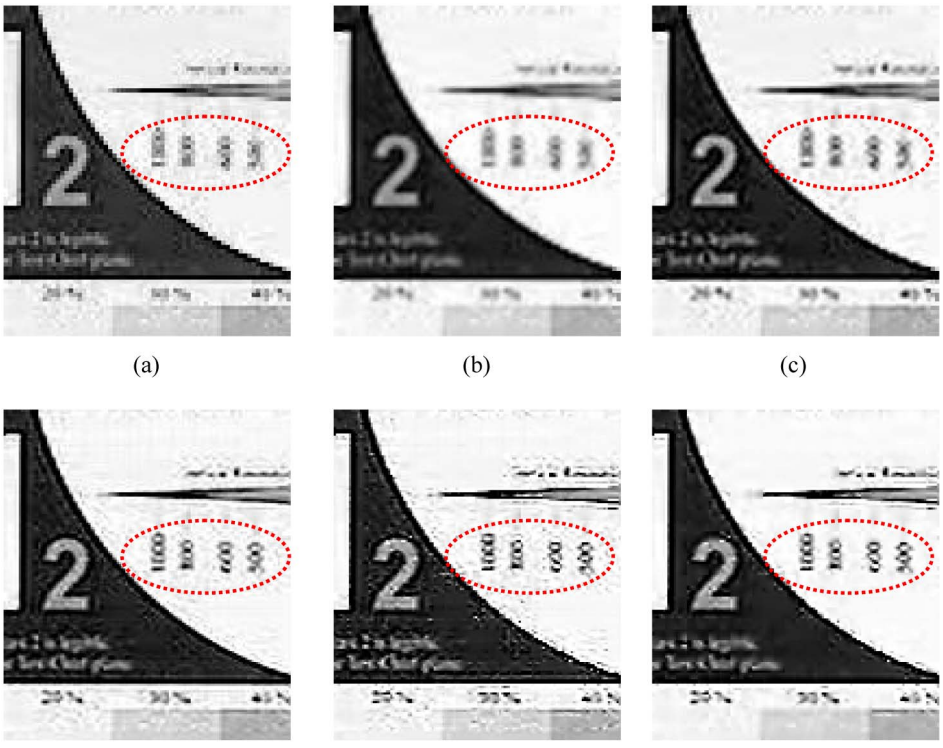

(a) (b) (c)

(d) (e) (f)

Fig. 9. (Color online) Reconstruction results of the third experiment. (a) LR image. (b) Bilinear interpolation. (c) Bi-cubic interpolation. (d) Laplacian prior result. (e) Huber-MRF prior result. (f) Proposed LSA result.

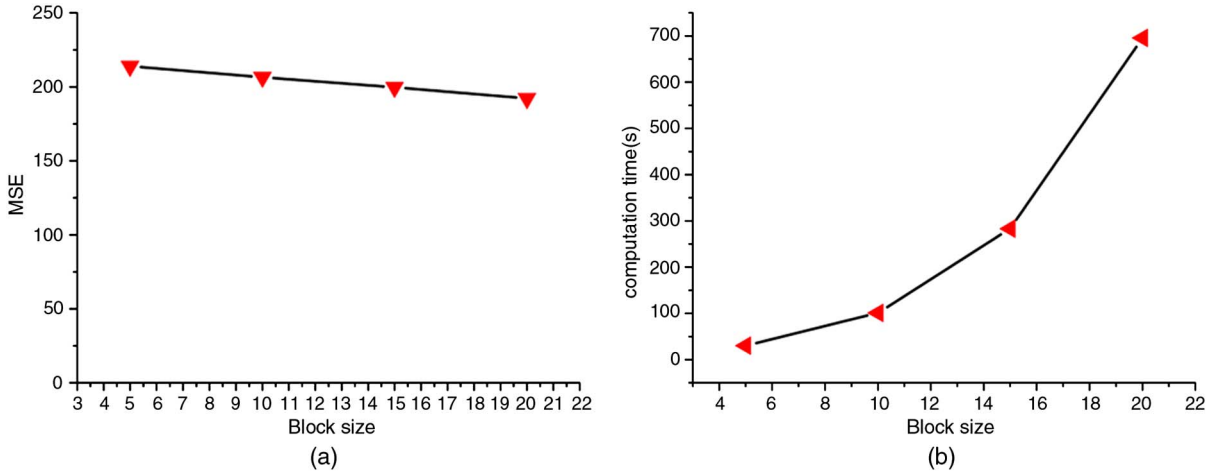

Fig. 10. (Color online) Change in the MSE and computation time versus block size in the first experiment (a) The change of the MSE value versus block size (b) The change of the computation time versus block size.

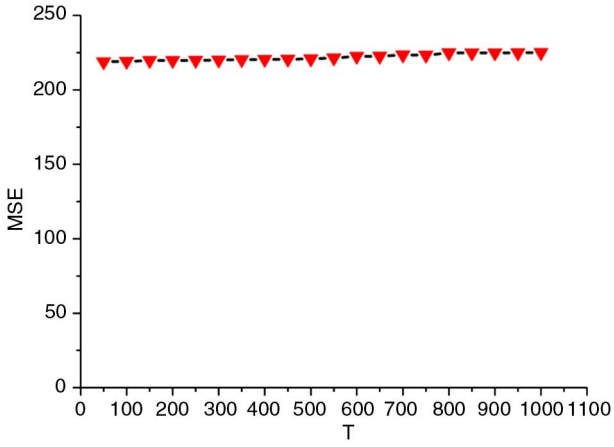

Fig. 11. (Color online) Change in the MSE value versus the threshold parameter T in the first experiment.

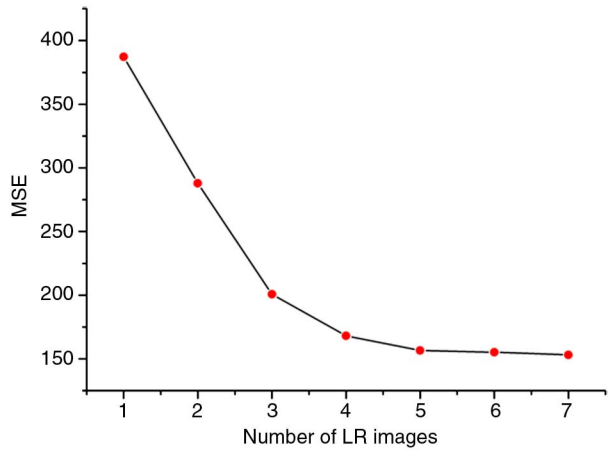

Fig. 12. (Color online) Change in the MSE value versus the number of LR images.

Figure 11 provides a plot showing the change in the MSE value with the parameter T from 50 to 1000 in the first experiment. It is found that the MSE of the reconstruction result has little change with the change of the parameter T from 50 to 1000, which illustrates that a good reconstruction result is possible, as long as the parameter T is set in some range. One simple way to select T may be to plot the distribution histogram of the parameter δ_m of each block and select the inflection point as the threshold T.

The number of LR frames plays a very important role in the super-resolution process. In [48], the authors offer some conclusions about how to set a sufficient number of LR images with the magnification factor. They concluded that when the magnification factor was an integer M, the sufficient number of LR images was M^2. In our paper, because the magnification factor in all the experiments is set to 2, the number of LR images is sufficiently set to be around 4. In Fig. 12, the relationship between the LR frames and the reconstruction MSE values has been given to illustrate the sufficient number of the LR images. It can be clearly seen that the LR image number is sufficient to be set as 4, which agrees with the conclusion in [48].

6. CONCLUSION AND FUTURE RESEARCH

In this paper, we present a local spatially adaptive super-resolution method, in which the prior model and the regularization parameter are adaptively selected according to the spatial characteristics of different parts of the image. To realize the local spatially adaptive process of the prior model, the structure tensor is used to identify the properties of different parts of the HR image. The Laplacian prior is used in the smoother parts to suppress noise and maintain the partial smoothness, and the Huber-MRF prior is used in rougher areas to preserve the edge information. Meanwhile, a relationship between the regularization parameter and the spatial information is constructed to realize the local adaptive process of the regularization parameter. A large regularization parameter is selected in smoother areas to suppress noise, while a small parameter is selected in the nonsmooth areas to preserve edge information. A set of experiments showed that the proposed approach achieves better reconstruction results than conventional methods, both in visual effects and in quantitative terms.

Although the proposed approach works well, it also has some areas to be improved, such as in experiment 3, where

a small distortion effect is produced in the lower left corner of the super-resolution results. We think that this distortion may be attributable to the following reasons: (1) although the registration method used in this paper produces good result, registration error also exists, which will produce distortion; (2) the "Surveillance" video sequence used in experiment 3 has considerable compression noise, which again will produce distortion.

Therefore, in future research, we will focus on researching a more accurate registration algorithm and consider the compression process in the degradation process of the HR image, in order to pursue a further improved reconstruction result.

ACKNOWLEDGMENTS

We appreciate the helpful comments and sugestions from the editors and reviewers. This work was supported by the Major State Basic Research Development Program (973 Program) of China under grant no. 2011CB707103; the National Natural Science Foundation of China under grant nos. 40930532, 40801182, 40971220, 41071269, and 41010082; the Research Fund for the Doctoral Program no. 200804861006; the National High Technology Research and Development Program (863 Program) of China under grant no. 2009AA12Z114; and the Program for New Century Excellent Talents in University under grant NECT-10-0624.

REFERENCES

1. R. Y. Tsai and T. S. Huang, "Multi-frame image restoration and registration," Adv. Comput. Vision Image Process. **1**, 317–339 (1984).
2. S. P. Kim, N. K. Bose, and H. M. Valenzuela, "Recursive reconstruction of high resolution image from noisy undersampled multiframes," IEEE Trans. Acoust. Speech Signal Process. **38**, 1013–1027 (1990).
3. S. P. Kim and W. Y. Su, "Recursive high-resolution reconstruction of blurred multiframe images," IEEE Trans. Image Process. **2**, 534–539 (1993).
4. N. K. Bose, H. C. Kim, and H. M. Valenzuela, "Recursive implementation of total least squares algorithm for image reconstruction from noisy, undersampled multiframes," *Proceedings of IEEE Conference on Acoustics, Speech and Signal Processing* (IEEE, 1993), pp. 269–272.
5. H. Ur and D. Gross, "Improved resolution from sub-pixel shifted pictures," CVGIP: Graph. Models Image Process **54**, 181–186 (1992).
6. M. S. Alam, J. G. Bognar, R. C. Hardie, and B. J. Yasuda, "Infrared image registration and high-resolution reconstruction using multiple translationally shifted aliased video frames," IEEE Trans. Instrum. Meas. **49**, 915–923 (2000).
7. M. Irani and S. Peleg, "Improving resolution by image registration," CVGIP: Graph. Models Image Process. **53**, 231–239 (1991).
8. M. Irani and S. Peleg, "Motion analysis for image enhancement resolution, occlusion, and transparency," J. Visual Commun. Image Represent. **4**, 324–335 (1993).
9. R. Gonsalves and F. Khaghani, "Super resolution based on low-resolution, warped images," Proc. SPIE **4790**, 10–20 (2002).
10. H. Stark and P. Oskoui, "High-resolution image recovery from image plane arrays, using convex projections," J. Opt. Soc. Am. A **6**, 1715–1726 (1989).
11. A. J. Patti, M. I. Sezan, and A. M. Tekalp, "Super resolution video reconstruction with arbitrary sampling lattices and nonzero aperture time," IEEE Trans. Image Process. **6**, 1064–1076 (1997).
12. R. C. Hardie, K. J. Barnard, J. G. Bognar, E. E. Armstrong, and E. A. Watson, "High-resolution image reconstruction from a sequence of rotated and translated frames and its application to an infrared imaging system," Opt. Eng. **37**, 247–260 (1998).
13. B. C. Tom and A. K. Katsaggelos, "Reconstruction of a high-resolution image by simultaneous registration, restoration, and interpolation of low-resolution images," *Proceedings of 1995 IEEE International Conference on Image Processing* (IEEE, 1995), pp. 539–542.
14. M. Elad and A. Feuer, "Restoration of a single superresolution image from several blurred, noisy, and undersampled measured images," IEEE Trans. Image Proc. **6**, 1646–1658 (1997).
15. R. R. Schulz and R. L. Stevenson, "Extraction of high-resolution frames from video sequences," IEEE Trans. Image Process. **5**, 996–1011 (1996).
16. R. C. Hardie, K. J. Barnard, and E. E. Armstrong, "Joint MAP registration and high-resolution image estimation using a sequence of undersampled images," IEEE Trans. Image Process. **6**, 1621–1633 (1997).
17. H. Shen, L. Zhang, B. Huang, and P. Li, "A MAP approach for joint motion estimation, segmentation and super-resolution," IEEE Trans. Image Process. **16**, 479–490 (2007).
18. N. A. Woods, N. P. Galatsanos, and A. K. Katsaggelos, "Stochastic methods for joint registration, restoration, and interpolation of multiple undersampled images," IEEE Trans. Image Process. **15**, 201–213 (2006).
19. L. C. Pickup, D. P. Capel, S. J. Roberts, and A. Zisserman, "Bayesian methods for image super-resolution," Comput. J. (UK) **52**, 101–113 (2008).
20. M. Protter, M. Elad, H. Takeda, and P. Milanfar, "Generalizing the nonlocal-means to super-resolution reconstruction," IEEE Trans. Image Process. **18**, pp. 36–51 (2009).
21. Takeda, P. Milanfar, M. Protter, and M. Elad, "Super-resolution without explicit subpixel motion estimation," IEEE Trans. Image Process. **18**, pp. 1958–1975 (2009).
22. R. H. Chan, T. F. Chan, L. Shen, and Z. Shen, "Wavelet algorithms for high-resolution image reconstruction," SIAM J. Sci. Comput. **24**, 1408–1432 (2003).
23. M. K. Ng, C. K. Sze, and S. P. Yung, "Wavelet algorithms for deblurring models," Int. J. Imaging Syst. Technol. **14**, 113–121 (2004).
24. N. Nguyen and P. Milanfar, "A wavelet-based interpolation restoration method for superresolution (wavelet superresolution)," Circuits, Systems, Signal Process. **19**, 321–338 (2000).
25. H. Ji and C. Fermuller, "Robust wavelet-based super-resolution reconstruction: theory and algorithm," IEEE Trans. Pattern Anal. Mach. Intell. **31**, 649–660 (2009).
26. S. C. Park, M. K. Park, and M. G. Kang, "Super-resolution image reconstruction: a technical overview," IEEE Signal Process. Mag. **20**, 21–36 (2003).
27. S. Farsiu, M. D. Robinson, M. Elad, and P. Milanfar, "Fast and robust multi-frame super resolution," IEEE Trans. Image Process. **13**, 1327–1344 (2004).
28. S. Farsiu, M. D. Robinson, M. Elad, and P. Milanfar, "Advances and challenges in super-resolution," Int. J. Imaging Syst. Technol. **14**, 47–57 (2004).
29. A. K. Katsaggelos, R. Molina, and J. Mateos, *Super Resolution of Images and Video* (Morgan and Claypool, 2007).
30. S. Chaudhuri, Ed., *Super-Resolution Imaging* (Kluwer, 2001).
31. P. Milanfar, *Super Resolution imaging* (CRC Press, 2010).
32. L. C. Pickup, "Machine learning in multi-frame image super-resolution," Ph.D. (University of Oxford, 2007).
33. M. K. Ng, H. Shen, E. Y. Lam, and L. Zhang, "A total variation regularization based super-resolution reconstruction algorithm for digital video," EURASIP J. Adv. Signal Process. Article ID 74585 (2007).
34. T. G. Stockman, "Image processing in the context of a visual model," Proc. IEEE **60**, 828–842 (1972).
35. T. Peli and J. S. Lim, "Adaptive filtering for image enhancement," Opt. Eng. **21**, 108–112 (1982)
36. H. Su, L. Tang, D. Tretter, and J. Zhou, "A practical and adaptive framework for super-resolution," *Proceedings of IEEE International Conference on Image Processing 1* (IEEE, 2008), pp. 1236–1249.
37. J. Lim, "Image restoration by short space spectral subtraction," IEEE Trans. Acoust. Speech Signal Process. **28**, 191–197 (1980).

38. X. Zhang and K.-M. Lam, "Image magnification based on a block-wise adaptive Markov random field model," Image Vision Comput. **26**, 1277–1284 (2008).
39. R. Pan and S. J. Reeves., "Efficient Huber-Markov edge-preserving image restoration," IEEE Trans. Image Process. **15**, 3728–3735 (2006).
40. W. Forstner and E. Gulch, "A fast operator for detection and precise location of distinct points, corners and centres of circular features," *Proceedings ISPRS Intercommission Conference on Fast Processing of Photogrammetric Data* (Academic, 1987), pp. 281–305.
41. J. Bigun and G. H. Granlund, "Optimal orientation detection of linear symmetry," *Proceedings First International Conference on Computer Vision* (IEEE, 1987), pp. 433–438.
42. T. Brox, J. Weickert, B. Burgeth, and P. Mrázek, "Nonlinear structure tensors," Image Vis. Comput. **24**, 41–55 (2006).
43. G. H. Golub and C. F. van Loan, *Matrix Computation*, 3rd ed. (Johns Hopkins University Press, 1996)
44. H. Shen and L. Zhang, "A MAP-based algorithm for destriping and inpainting of remotely sensed images," IEEE Trans. Geosci. Remote Sens. **47**, 1492–1502 (2009)
45. P. Vandewalle, S. Susstrunk, and A. Vetterli, "A frequency domain approach to registration of aliased images with application to super-resolution," EURASIP J. Appl. Signal Process., Article ID 71459 (2006).
46. Z. Wang, A. C. Bovik, and H. R. Sheikh, "Image quality assessment: from error visibility to structural similarity," IEEE Trans. Image Proc. **13**, 600–612 (2004).
47. http://users.soe.ucsc.edu/~milanfar/software/sr-datasets.html
48. Z. Lin and H. Shum, "Fundamental limits of reconstruction-based superresolution algorithms under local translation," IEEE Trans. Pattern Anal. Mach. Intell. **26**, 83—97 (2004).